Journal of Advanced Engineering Research
ISSN: 2393-8447
Volume 9, Issue 1, 2022, pp.29-34

Tribological studies on the lubrication properties of journal bearing

Arjun Sikka[1*], Nitin Sharma[1]

[1]Department of Mechanical Engineering, Dr BR Ambedkar National Institute of Technology, Jalandhar, India 144027

*Corresponding author email: arjuns.te.21@nitj.ac.in, Tel. :9501588994

ABSTRACT

In rotating machinery, such as turbines and internal combustion engines, journal bearings are commonly utilized. Problems can be prevented and time-to-market can be shortened with the capacity to examine bearing behavior early in the product development process (PDP). The finite difference method (FDM) is used as a numerical technique in this work to create a simulation tool for journal bearings in MATLAB software. The simulation tool may serve as a virtual test rig to examine bearing performance in terms of pressure distribution, fluid film thickness, load carrying capability, and other parameters. The design of bearings is simplified further by this.

Keywords – Bearing, MATLAB, Sommerfeld boundary condition, Reynolds number.

1. INTRODUCTION

The automotive industry is today facing challenges with the increasing environmental priorities and the continuously changing customer needs. This has led to a significant change of companies' priorities and a greater focus on environmental policies. The adoption of an efficient product development process (PDP) has become crucial for companies to be able to reduce lead times. Hydrodynamic journal bearings are crucial elements to transmit force and reduce friction between two moving surfaces, where a shaft is rotating inside a fixed sleeve. Numerical analysis of hydrodynamic lubrication has allowed for close approximations of bearing characteristics. There exist several available numerical methods that have been developed, e.g. the finite difference method (FDM).

In 1883, B. Tower published a report with experimental results where the influence of lubrication on friction with surfaces submerged into an oil-bath had been investigated [1, 2]. In 1886, O. Reynolds presented a partial differential equation (PDE) describing the pressure build-up in the lubrication film that occur in self-acting bearings. This equation made it possible to predict bearing performance and analyze how the bearing was going to operate under certain conditions [3-5].

Hydrodynamic theory gives an approximation of the pressure build-up and is often used while analyzing hydro dynamically lubricated bearings such as journal bearings. However, different bearing operating conditions, the use of gas-bearings and other bearing influencing factors called for another examination of the equation describing hydrodynamic lubrication. This led to the formulation of the so-called generalized Reynolds equation which permits variation of relevant quantities throughout the lubricant film.

When employing conventional lubricants, the hydrodynamic performance of a journal bearing may be described by a plot of the friction coefficient vs a non-dimensional load parameter known as a Stribeck curve. One of the curve's key features is that as the lubricant film thickness grows, the friction coefficient initially drops until it hits a minimum, then increases owing to lubricant film shearing. The experimental study describes additional experiments performed on a three-pad journal bearing employing tungsten disulfide powder as the lubricant to assess its heat stability and long-term wear characteristics. Lubricant made of dry tungsten disulfide powder has been shown to have good wear resistance. It has similar friction qualities to molybdenum disulfide, but it can withstand much greater temperatures [6]. Another study [7] examined the behavior of journal bearings made from polytetrafluoroethylene (PTFE) composites and aluminum (Al) alloys. The PTFE composites had a 1.6 mm steel backing, a 0.24-0.27 mm sintered porous bronze middle layer, and carbon fibers loaded with 11 fluorinated ethylene propylene (FEP) powder and carbon fiber. The Al alloy journal bearings showed excellent adhesion at loads ranging from 6300 to 8000 N. This shows that Al alloys are a better choice for journal bearings than PTFEs, according to the experimental data.

Journal bearing material wear was found to be higher in SAE 20W40 and CMRO. This research examines the tribological behavior of traditional materials such as Brass and Gunmetal, as well as a new nonmetallic material called Cast Nylon. Finding effective ecologically friendly lubricating fluids is a significant problem in addition to the ongoing quest to reduce wear. This research aims to evaluate the literature on wear and friction in hydrodynamic journal bearings in order to better understand current advances and trends in the field.

In 2013, G.V.Punna Rao, Y.Bhargavi, and A.Navanth[8] published a study proving that friction and wear management is essential for cost-effectiveness and durability. S.M. Muzakkir, K.P. Lijesh, and Harish Hirani[9] presented a report in 2014 in which they show that the possibility of hybridising a magnetic arrangement in a traditional journal bearing system has been tested under heavy load and slow speed working circumstances. Journal bearings and other lubricated machine parts rely heavily on the fluid's pressure condition, as shown by study by Chetan Mehra, Amar Singh Kokadiya, and Neelesh Khandare[10] in 2014. With the use of a pin on disc wear tester and three distinct lubricants, they studied the friction and wear behaviour of journal bearing material. Wear testing was conducted at 200 N maximum load and 2–10 m/s sliding speeds. For CMRO with Nano CuO, it has a lower friction coefficient than the other two oils. Only a well-designed slip surface can improve the tribological performance of journal bearings. The journal bearing serves as a support for high rotary speeds as well as a dampening element for high-speed vibration absorption. If lubrication fails or is starved in the hydrodynamic zone, it causes a great amount of friction between the shaft and bearing, resulting in severe wear loss and damage to the component's surfaces.

In 2018, V. R. Sagar, T. Mali, and M. Chewale[11] published a paper in which they show that when journal bearings are used in heavy-duty applications, lubricating oil degradation is accelerated. To improve the oil's thermal stability, dry particles are added to the lubricant. Graphite particles are an efficient additive found in Machinol 100 oil. To validate experimental data, they used Minitab's multiple regression approach to establish a link between the two sets of variables, and then conduct a conformation test to calculate the percentage of discrepancy between the two sets of results.

In 2018, Ahmed Mohamed Mahmoud Ibrahim, Ahmed Fouly Anwar Mohamed, Ahmed M R Fathelbab, and Fadl A Essa presented their findings in a study paper. [12] The research was conducted with the objective of developing novel materials that might one day successfully replace metals used in bearings. One further study[13] concluded that INCONEL 625 is the best material for journal bearings because of its low wear rate, absence of wear rate fluctuation, lowered coefficient of friction, and better mechanical properties. By the year 2020, research by N. Sharma and S. Kango[14] had shown how different geometric configurations affected tribological behavior. Researchers have shown that standard bearings' tribological qualities may be greatly enhanced by embedding surface textures of varying shapes and sizes (rectangular, triangular, square, spherical, elliptical, etc.) into the bearing surface. The goal of this study was to analyze the efficiency of porous journal bearings using spherical-shaped textures while taking into consideration the location of the textures at different eccentricity ratios (0.3 & 0.7).

2. METHODOLOGY

Following the application of the Reynolds equation to the journal bearing problem, it is subsequently discretized with the use of the Finite Difference Method and the Central Differencing Scheme. Following this step, Sommerfeld and Reynolds' Boundary Conditions are used in order to compute the pressure distribution that is associated with each boundary condition over the bearing surface. Pressure distribution and fluid film thickness fluctuation over the bearing surface may be calculated with the help of the discretized Reynolds Equation. The load carrying capacity is calculated by numerically integrating the pressure function across the bearing surface, which is obtained from Reynolds's equation. Simpson's 1/3 Rule is used for numerical integration.

2.1 Finite Difference Scheme

Differential equations may be approximated using finite differences for derivatives. In one dimension, L. Euler (1707–1783) made the discovery in 1768, while in two dimensions, C. Runge (1856–1927) made the advancement in 1908. In the early 1950s, finite difference methods were first used in numerical applications. The advent of computing provided a framework for tackling difficult problems in science and technology. Accuracy, stability, and convergence results for finite-difference methods for PDEs have been established theoretically in the past 50 years. By approximating derivatives, differential equations may be solved using finite-difference techniques (FDM). At

discrete locations, the solution is approximated by dividing the space-time coordinates into a finite number of steps.

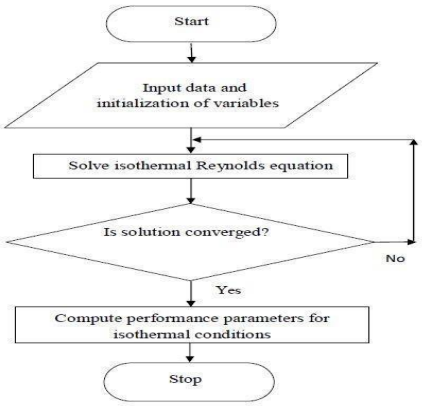

Figure 1. Solving the Reynolds equation numerically by using MATLAB software

2.2 Discretization

Finite Difference Method (Taylor Series Expansion)

$$f(x+\Delta x) = f(x) + \frac{\partial f}{\partial x}\Delta x + \frac{1}{2!}\frac{\partial^2 f}{\partial x^2}(\Delta x)^2 + \frac{1}{3!}\frac{\partial^3 f}{\partial x^3}(\Delta x)^3 + \ldots + \frac{1}{n!}\frac{\partial^n f}{\partial x^n}(\Delta x)^n + \ldots$$

First derivative

Second derivative

2.3 Finite Differencing of first derivative

Rearranging the Taylor series expansion yields the finite difference approximation for first-order derivatives as follows:

Forward: $$\left(\frac{\partial f}{\partial x}\right)_i = \frac{f_{i+1} - f_i}{\Delta x} + o(\Delta x)$$

Backward: $$\left(\frac{\partial f}{\partial x}\right)_i = \frac{f_i - f_{i-1}}{\Delta x} + o(\Delta x)$$

Central: $$\left(\frac{\partial f}{\partial x}\right)_i = \frac{f_{i+1} - f_{i-1}}{2\Delta x} + o(\Delta x)^2$$

Truncation Error

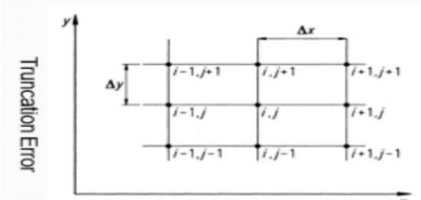

Figure 2. Truncation error in Finite Difference Scheme

2.4 Finite Differencing of second derivative

For second order finite differencing derivatives, we employ the Taylor series expansion. Second derivative approximations:

Central difference: $$\left(\frac{\partial^2 f}{\partial x^2}\right)_i = \frac{f_{i+1} - 2f_i + f_{i-1}}{(\Delta x)^2} + o(\Delta x)^2$$

Forward difference: $$\left(\frac{\partial^2 f}{\partial x^2}\right)_i = \frac{f_{i+2} - 2f_{i+1} + f_i}{(\Delta x)^2} + o(\Delta x)$$

Backward difference: $$\left(\frac{\partial^2 f}{\partial x^2}\right)_i = \frac{f_i - 2f_{i-1} + f_{i-2}}{(\Delta x)^2} + o(\Delta x)$$

First and second derivative approximations show that central differencing has the least truncation error $(\Delta x)^2$ This study uses Finite Difference using central differencing.

2.5 Discretizing the Reynold's Equation

The 2-Dimensional Reynolds equation is given below:

$$\frac{\partial}{\partial x}\left(h^3\frac{\partial p}{\partial x}\right) + \frac{\partial}{\partial z}\left(h^3\frac{\partial p}{\partial z}\right) = 6\eta U\frac{\partial h}{\partial x}$$

$$\frac{\partial}{\partial x}\left(h^3\frac{\partial p}{\partial x}\right) + h^3\frac{\partial}{\partial z}\left(\frac{\partial p}{\partial z}\right) = 6\eta U\frac{\partial h}{\partial x}$$

$$h^3\frac{\partial^2 p}{\partial x^2} + 3h^2\frac{\partial p}{\partial x}\frac{\partial h}{\partial x} + h^3\frac{\partial^2 p}{\partial z^2} = 6\eta U\frac{\partial h}{\partial x}$$

$$\frac{\partial^2 p}{\partial x^2} + \frac{\partial^2 p}{\partial z^2} = \left(-\frac{3}{h}\frac{\partial p}{\partial x} + \frac{6\eta U}{h^3}\right)\frac{\partial h}{\partial x}$$

2.6 Discretizing by central differencing

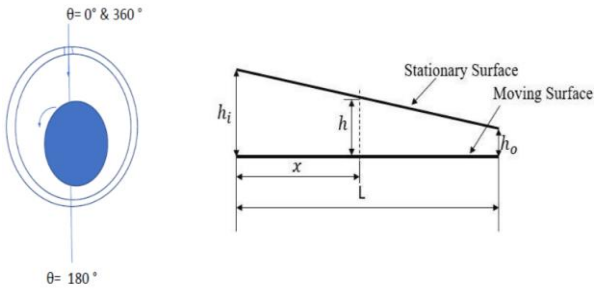

Figure 3. Oil Wedge forms between shaft/journal and bearing due to them not being concentric

$h = Cr\,(1 + \varepsilon*\cos\theta)$

$dx = R*d\theta$

$d\theta = 6.28/(Nx-1)$

$dz = L/(Nz-1)$

where Nx and Nz represent the total number of nodes in the x and z directions, respectively.

$$\frac{p(i+1,k)-2p(i,k)+p(i-1,k)}{dx^2}+\frac{p(i,k+1)-2p(i,k)+p(i,k-1)}{dz^2}=$$

$$\left(-\frac{3}{h}\frac{\partial p}{\partial x}+\frac{6\eta U}{h^3}\right)\frac{\partial h}{\partial x}$$

$$\frac{\partial p}{\partial x}=\frac{p(i+1,k)-p(i-1,k)}{2dx}=\text{A1 (i,k)}$$

$$\frac{\partial h}{\partial x}=\frac{h(i+1,k)-h(i-1,k)}{2dx}=A2(i,k)$$

$$\frac{6\eta U}{h^3}=\frac{6\eta U}{(h(i,k))^3}=A3(i,k)$$

$$\frac{3}{h(i,k)}=A4(i,k)$$

$$\frac{p(i+1,k)+p(i-1,k)}{dx^2}=A5(i,k)$$

$$\frac{p(i,k+1)+p(i,k-1)}{dz^2}=A6(i,k)$$

$$A7=\frac{2}{dx^2}+\frac{2}{dz^2}$$

The Resulting equation becomes:

A5(i,k) + A6(i,k) – A7*p(i,k) =
(A4(i,k)*A1(i,k)+A3(i,k))*A2(i,k)

The pressure profile is given by:

p(i, k) = −(1/A7){[(−A4(i, k)A1(i, k) +
A3(i,k))A2(i, k)] − A5(i, k) − A6(i, k)}

Two-dimensional Reynolds' Equation is discretized using central differencing. MATLAB code is developed using the above discretization. This code calculates pressure and film thickness.

2.7 Boundary Conditions

Full Sommerfeld Boundary Condition

(i) p = 0 at θ = 0
(ii) p(0) = p(2π)

This indicates that the film is full (i.e upto 2π)

Half Sommerfeld Boundary Condition

(i) p = 0 at θ = 0
(ii) p = 0 at $\pi \le \theta \le 2\pi$

Reynold's Boundary Condition

(i) p = 0 at θ = 0
(ii) p = 0 at $\theta_2 \le \theta \le 2\pi$ ($\theta_2 > \pi$)
(iii) $dp/d\theta = 0$ at $\theta = \theta_2$

The pressure distribution across the bearing surface is calculated by solving the Reynold's equation according to the aforementioned boundary conditions. A graph of the mid-plane pressure readings vs the angle in degrees is then constructed.

2.8 Load-carrying capacity calculation from Reynolds Equation

The load capacity of the lubricating film is determined by integrating the bearing pressure distribution. When the load is changed, the film shape also adjusts, rebalancing the load and pressure. At a certain film geometry, the bearing may support:

$$W=\int_0^L\int_0^B p\,dx\,dy$$

In order to optimize operational and design characteristics, the load formula is specified in terms of bearing geometry, lubricant viscosity, and speed.

In this study, the load bearing capacity is calculated numerically using Simpson's 1/3 method.

2.9 Simpson's 1/3rd Rule of numerical integration:

Simpson's 1/3rd rule for double integration is given below:

$$I=\frac{hk}{9}\left\{\begin{matrix}[f(x_{i-1},y_{j-1})+4f(x_{i-1},y_j)+f(x_{0i-1},y_{j+1})]+4[f(x_i,y_{ij-1})+4f(x_j,y_j)+f(x_i,y_{j+1})]+\\ f(x_{i+1},y_{j-1})+4f(x_{i+1},y_j)+f(x_{j+1},y_{j+1})\end{matrix}\right\}$$

The pressure function derived by finite differencing of Reynolds' Equation is used in conjunction with Simpson's 1/3 Rule of Numerical Integration to determine the load-carrying capacity.

Then the load capacity at different eccentricity ratios is calculated and a graph is plotted between them.

2.10 Validation of the work

The model is validated by applying all of the parameters (equations, input variables, etc.) derived from Sharma N.'s work [9].

All the values from the work of Sharma N [9] like eccentricity ratio, bearing dimensions are given as input to the MATLAB program and results are compared with the experimental results.

3. RESULTS AND DISCUSSION

Using the discretized Reynolds Equation, pressure distribution and fluid film thickness variation are obtained. Integrating the pressure function across the bearing surface gives the Load Carrying Capacity.

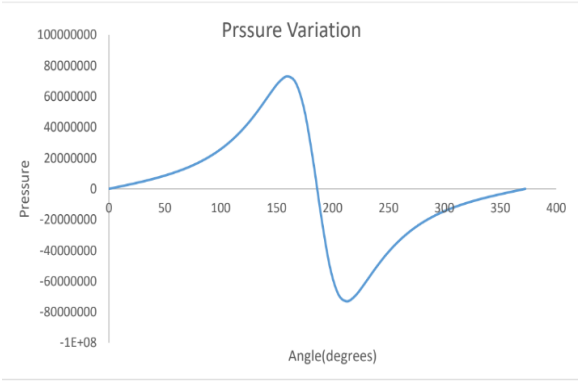

Figure 4. Plot of Pressure v/s Angle(degrees) for full Sommerfeld condition

The above figure is a graph between the mid plane pressure values and the angle in degrees.
These values are for Full Sommerfeld Boundary Condition:

(i) $p = 0$ at $\theta = 0$

(ii) $p(0) = p(2\pi)$

This indicates that the film is full (i.e upto 2π)

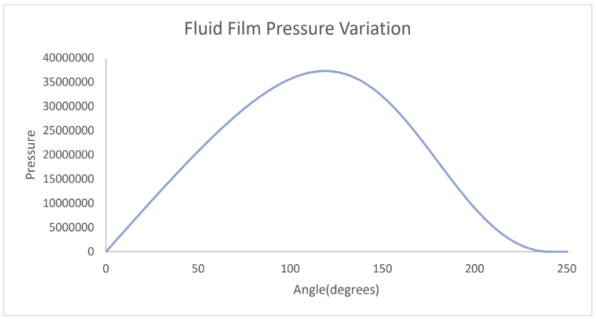

Figure 5. Plot of Pressure v/s Angle(degrees) for Reynold's Boundary condition

The above figure is a graph between the mid plane pressure values and the angle in degrees.
These values are for Reynold's Boundary Condition:
(i) $p = 0$ at $\theta = 0$
(ii) $p = 0$ at $\theta_2 \leq \theta \leq 2\pi$ ($\theta_2 > \pi$)
(iii) $dp/d\theta = 0$ at $\theta = \theta_2$
In order to satisfy the full Sommerfeld Boundary Condition, a positive pressure must be generated in the convergent film ($0 \leq \theta \leq \pi$) and a negative pressure must be generated in the divergent film ($\pi < \theta < 2\pi$). There is no discernible asymmetry in the distribution of pressure.
The pressures obtained from full Sommerfeld condition in the divergent film region are negative (less than ambient pressure). Such conditions are rarely encountered in real bearings.
In Reynold's Boundary Condition the pressure becomes zero at some $\theta_2 > \pi$. Thus, Reynold's Boundary Condition is more realistic.

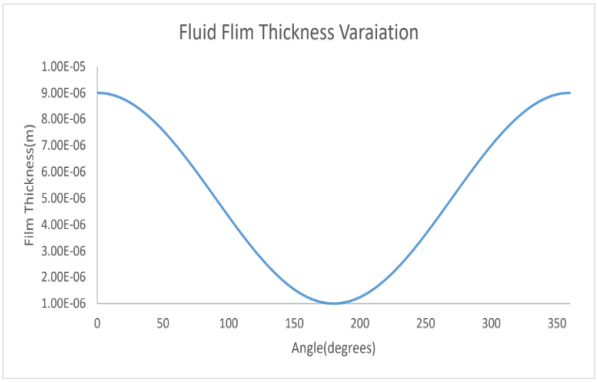

Figure 6. Plot of fluid film thickness (m) v/s Angle (degrees)

The above figure represents fluid film thickness (m) variation with angle (in degrees)
For a given rotational velocity, the pressure builds up to a point where the load can be supported at the closest approach between the journal and the bearing, when the fluid film thickness is at its lowest. When the minimal fluid film thickness exceeds the amount based on the nature of the roughness of the contacting surfaces, complete lubrication is achieved.

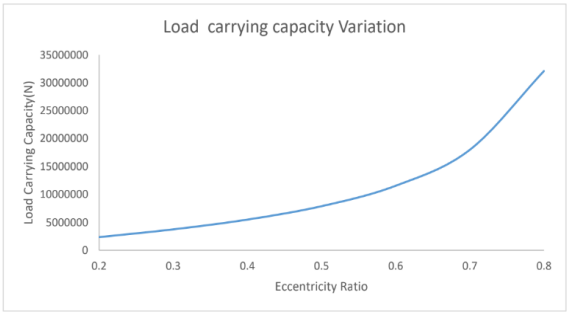

Figure 7. Plot of Load Carrying Capacity (N) v/s Eccentricity Ratio

Figure 7 represents the graph between load-carrying capacity and eccentricity ratio. With an increased eccentricity ratio, the bearing is subjected to a heavier external load. The graph clearly shows that when eccentricity ratio rises, load bearing capability rises as well.
A greater eccentricity ratio (0.7-0.8) results in a faster rate of growth.

5. CONCLUSION

Using the Reynolds equation and several boundary conditions, including the Sommerfeld and Reynolds boundary conditions, a numerical model has been developed in this study. For the purpose of simulation, a MATLAB code has been written. The current numerical model was developed for use in a finite journal bearing analysis. This paves the way for a study of critical

bearing performance metrics such fluid film thickness, load capacity, and pressure distribution. By comparing the model's pressure variation findings with those of earlier studies utilizing Reynolds and Sommerfeld boundary conditions, we find that the model is robust. The findings show that the load-carrying capacity grows steadily with increasing eccentricity ratio values, and especially rapidly at large eccentricity ratios (0.7-0.8).

REFERENCES

[1] A. van Beek, *Advanced Engineering Design*, Delft: TU Delft, 2012.

[2] B. Tower, *"First report on friction experiments," vol. 34, no. 1*, 1883, 632-659.

[3] O. Reynold, "On the Theory of Lubrication and Its Application to Mr. Beauchamp Tower's Experiments, Including an Experimental Determination of the Viscosity of Olive Oil.," *Proceedings of the Royal Society of London, vol. 40(242-245)*, 1886, 191-203.

[4] B. J. Hamrock, *Fundamentals of fluid film lubrication*, New York: McGraw-Hill, 1994.

[5] D. Dowson, "A generalized Reynolds equation for fluid-film lubrication," *International Journal of Mechanical Sciences, 4(2)*, 1962, 159-170.

[6] H. Heshmat, D. E. Brewe, Performance of a Powder Lubricated Journal Bearing With WS2 Powder: Experimental Study. *J. Tribol. Jul 1996, 118(3)*: 484-491

[7] Boncheol Ku et al Comparison of tribological characteristics between aluminum alloys and polytetrafluoroethylene composites journal bearings under mineral oil lubrication. *Journal of Mechanical Science and Technology ,2010, Volume 8*, 1631-1635

[8] G.V.Punna Rao , Y.Bhargavi , A.Navanth A Recent Approach to Wear Concept in Hydrodynamic Journal Bearings , *International Journal 0f Engineering And Science ,2013 ,Vol. 3*, 83-94.

[9] S.M. Muzakkir K.P. Lijesh, Harish Hirani Tribological failure analysis of a heavily-loaded slow speed hybrid journal bearing. *Engineering Failure Analysis 2014, 40*,97-113.

[10] Chetan Mehra, Amar Singh Kokadiya, Neelesh Khandare. Study of Pressure Profile in Hydrodynamic Lubrication Journal Bearing... International Journal of Engineering Research & Technology (IJERT), 2014, Vol. 3 Issue 7, 359-362.

[11] V. R. Sagar, T. Mali, M. A. Chewale. An Experimental Study of Tribological Behaviour of Journal Bearing Material under Dry Lubrication… *International Journal of Advance Research in Science and Engineering, 2018 Volume -7* , 302-311

[12] Ahmed Mohamed Mahmoud Ibrahim, Ahmed Fouly Anwar Mohamed, Ahmed M R Fathelbab and Fadl A Essa Enhancing the tribological performance of epoxy composites utilizing carbon nano fibers additives for journal bearings Materials *Research Express*, 2018, *Volume 6, Number*.

[13] Senkathir, A C Arun Raj, Shyamsunder R, Kameshwaran J, Nagu Aravind N S. Selection of Suitable Material for Journal Bearing by Tribology. *International Journal of Recent Technology and Engineering 2020. Volume-8* , 4392-4399

[14] N. Sharma, S. Kango Influence of High Permeability Parameter on the Performance of Textured Porous Journal Bearings. *Tribology in Industry, 2020*, 1-15.